Separation Between Coal and Gangue Based on Infrared Radiation and Visual Extraction of the YCbCr Color Space

REFAT MOHAMMED ABDULLAH ESHAQ[ID][1,2], **ERYI HU**[ID][1,2], **MENGGANG LI**[ID][1,2], **AND MURAD SALEH ALFARZAEAI**[ID][3]

[1]School of Mechanical and Electrical Engineering, China University of Mining and Technology, Xuzhou 221116, China
[2]Jiangsu Collaborative Innovation Center of Intelligent Mining Equipment, China University of Mining and Technology, Xuzhou 221116, China
[3]School of Computer Science and Technology, China University of Mining and Technology, Xuzhou 221116, China

Corresponding author: Eryi Hu (hu@cumt.edu.cn)

ABSTRACT Distinguishing between coal and gangue in the production lines of mining factories based on the thermal energy and infrared radiation emission of an object is feasible. In this paper, we use an infrared camera (IC) to distinguish between coal and gangue in the industrial mining field. Additionally, this system is considered to be a binary classification system that has two classes. We analyze the infrared images of coal and gangue; then extract the appropriate texture features from the infrared images in order to develop an accurate classification system by using support vector machine (SVM). The method applied in this work essentially depends on feature extraction of images. The statistical features based on gray level information (GLI), grey-level cooccurrence matrix (GLCM) and visual features are executed. Thus, we suggest preparation steps to obtain one select feature before importing the data into the SVM classifier, and this approach is adopted as the fundamental basis for our work. We exploit only one feature of the infrared image, namely, Cb, which is extracted from the YCbCr color space, and then compute the mean value of Cb after heating and capturing the photos for the coal and gangue samples. The proposed method achieves a high classification accuracy 97.83 % by using Gaussian-SVM.

INDEX TERMS Industrial mining, infrared camera application, gangue recognition, emissive power, YCbCr, SVM.
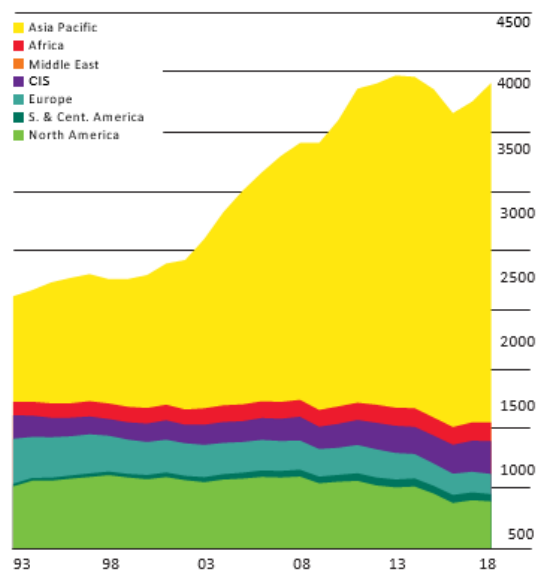
I. INTRODUCTION

Although coal is an environmental pollutant, it is still a valuable and indispensable resource, especially in producing thermal energy for affordable electrical energy. In the current century, many countries have been dramatically increasing mining prospects due to the reduction in worldwide oil and gas reserves and the increased global energy consumption, as presented in Fig. 1 [1]. Thus, the effectiveness and efficiency of coal production has been given priority by the largest developing countries. However, there are some drawbacks, such as the extraction rate of coal resources and the

The associate editor coordinating the review of this manuscript and approving it for publication was Jihwan P. Choi[ID].

percentage of rock content [2]. Moreover, both the dangers and poor detection rate of X-rays, which are utilized in identifying coal and gangue to separate them, in addition to ultraviolet light, which is used for the same purpose, are unsolved [3], [4].

Because of the hazards of X-ray and ultraviolet light, high maintenance cost and poor quality of classification of digital cameras, we suggest a new method for the separation of gangue from coal by incorporating an IC into the discrimination system. Before the manipulators select an unwanted object to remove it, as shown in Fig. 2, we should pass the wanted and unwanted objects through a wind heater such that the surface of the object acquires the same thermal energy between 30°C and 50°C, depending on the background

temperature. Then, the IC takes a photo of each object, and the variation will be obviously salient in the infrared image according to the law of heat transfer, particularly in terms of the infrared radiation energy; consequently, the manipulators make a decision based on data that are extracted from the infrared image, which we discuss in detail in this paper.

II. RELATED WORK

The field of coal mining is attracting many researchers and scholars. Yaqun, *et al.* [5] proposed the identification of coal and waste rock by using principal component analysis (PCA) and combined genetic neural network (GA-ANN). The authors acquire 100 % identification rates for gangue [5]. Coal–rock interface detection (CID) has been suggested by Sun and Su [2]; the method uses the texture features of images to discriminate between coal and rock samples [2]. The authors highlighted twenty-two texture features that were extracted from coal and rock images and then decreased the

data dimension from 22 to 4 by employing feature selection, which is considered the fundamental piece of their research [2]. Using this technique, the researchers reached an average recognition rate of 94.12 %, and they reduced the time complexity [2]. Gao *et al.* [6] developed a method to separate coal and gangue by using RGB components by making the mean grayscale value of coal and gangue images a key factor for the related neighborhood pixels recognition algorithm (RNRA). With that method, the authors achieved an accuracy of 96.8 % [6]. A method based on geometric, grayscale and texture feature of images was presented by Liu *et al.* [3]; the method exploits the multifractal detrended fluctuation analysis (MFDFA) method for extracting the geometric features and then applies the k nearest neighbor (kNN) algorithm in order to optimize the recognition rate. The recognition rate in that method successfully increased to 97.5 % [3] compared with that in [2]. Zhao *et al* [7], [8] proposed an identification method for a sorting system based on the statistical features of coal and gangue images; the method computes the statistical mean of each feature parameter based on GLI, such as the maximum value, mean value, variance, uniformity, smoothness and slope value. Based on the results of the statistical mean that were obtained in [7], Zhao [8] incorporated, the grayscale information with texture features into an intelligent sorting system by using an SVM recognition algorithm; the recognition rate for coal and gangue was greater than 81 % [8]. A convolutional neural network (CNN) method was discussed by Su *et al.* [9]; it improved the classic convolutional neural network (LeNet-5) through additional steps. Effectively, in that paper, the attained recognition rate was 95.88 %. Li and Sun [10] presented a recognition system for coal and gangue samples in which the authors utilized the least square support vector machine (LS-SVM) as a classifier. Before the data were input into the LS-SVM, two gray level features, the mean and peak of the grayscale, together with two texture features, the contrast ratio and entropy, had been selected as the feature vectors for the LS-SVM algorithm [10]. The obtained accuracy of that technique was 96.6 % for gangue and 98.7 % for coal [10]. Hu *et al.* [4] suggested a new method for the discrimination of coal and gangue by using multispectral imaging (MSI). The authors captured multispectral images for coal and gangue samples and then extracted features such as the histogram of oriented gradient (HOG), local binary pattern (LBP) texture feature vector and Haar feature (HAAT). Then, these authors imported the data set into the SVM classifier. A test accuracy of 96.25 % was successfully obtained [4]. Table 9 summarize all of the previous approaches.

Even though all those works successfully achieved a high recognition rate and accuracy, they have disadvantages. One shortcoming of the classification process is that it takes place when the illumination is diversified, which significantly affects the gray level information (GLI) and grey-level cooccurrence matrix (GLCM) for the image [8], [11]. We will also demonstrate this point experimentally in section V-*C*. Taking into consideration that the light changes with time,

there are many external and internal factors in mining factories that influence the intensity of light. The external factors include that the illumination in the morning is not the same as that in the afternoon, and sunny days are different from cloudy days, for example. The internal factors include that the quality of the lamp "source of light" or light-emitting diode (LED) inside mining factories deteriorates with time due to existing coal dust and haze (a slight obscuration of factory environment, typically caused by fine suspended particles lead to obstruct the visible light) in factories; in addition, these factors impact the lens of digital and multispectral cameras. A digital camera sensor has a wavelength sensitivity that ranges from approximately 0.35μm to 0.74μm [12]. Therefore, a small change in the intensity of light are detected by digital or multispectral cameras [12]. Consequently, the values of the texture feature "data set" will be completely unstable. Assuming that we design a classification system that depends on the extraction of texture features from images by using a digital or multispectral camera under a light intensity of 500 lux, if the light intensity decreases to 350 lux owing to the external or internal factors that we mentioned above, the classifier will not be able to recognize any sample. Therefore, the whole system will be ineffective [8]. Furthermore, the deposition of coal dust on the surface of gangue completely impacts the extracted feature value based on either GLCM or GLI. In addition, there is a large time complexity due to many features being selected for the separator function. Moreover, the experimental datasets, especially test images, are too small in some previous studies to yield conclusive results e.g., the experimental study conducted on only 20 samples of coal and gangue as test set presented in [5]. In addition, only 80 images are used as the test set in [4]. Additionally, 75 images for coal and 75 images are used as the test set in [10]. Therefore, the reliability of the results is poor. According to the norms of machine learning, the test set should be isolated from the training set. Additionally, the test set should be equal to or exceed the training set to avoid overfitting of the training model that are caused by optimized hyperparameters in the SVM during the training process [13]. Consequently, the accuracy of the test set "test images" is more important than that of the training set "training images"; thus, the number of test images should be considered.

In this paper, an IC is employed to improve upon previous works and to develop an optimum classification system with reliable results. Not only is the IC very safe but also it is an economical process in industrial mining to separate coal from gangue by using the manipulator. The IC is a sensor that detects the infrared radiation that is emitted by an object and converts it into a digital image that appears as high-contrast color from black to white. Additionally, the IC will help to increase the efficiency and decrease the cost of coal production by replacing or augmenting the human eye with other technology in order to reach optimum coal production in industrial mining. As mentioned above, light, dust and haze are critical in the field applications of coal and gangue
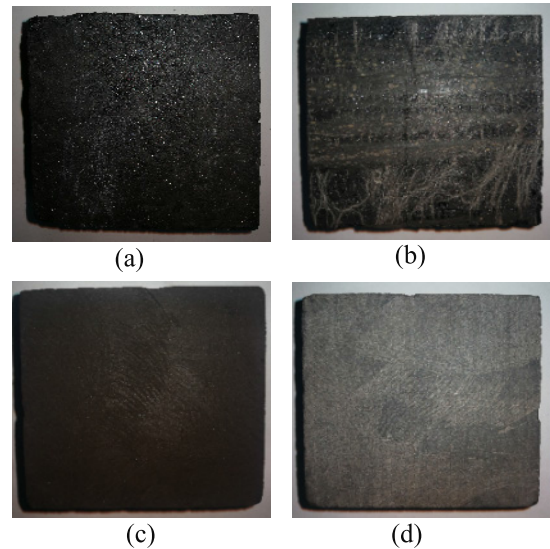

FIGURE 3. (a) is Coal, (b) is Mix, (c) is Black rock and (d) is Gray rock.

classification that use industrial digital cameras or multispectral cameras, and there are difficulties in applying the previously presented methods in practical environments; therefore, use of an IC is suggested. The significant advantages of an IC include that it can work in light or very dark environments with the same efficiency and yield high performance despite the change in the surface temperature. Additionally, dust, haze and light intensity are unable to impact or change the value of texture features of infrared images because the sensor of the IC operates in a spectral band ranging from 2μm to 14μm outside visible light. Moreover, the infrared radiation can pass through dust, haze and gases with very small losses, which can be considered negligible compared to visible light; this is called a **surface phenomenon** [14]. This point is experimentally proved in this paper. A **surface phenomenon** is the ability of an electromagnetic wave to pass an obstacle, e.g., gas, liquid and solid [14]. This phenomenon should be considered in the field of coal and gangue image classification when predominately using digital images or multispectral cameras.

III. MATERIALS AND METHODS
A. SAMPLE COLLECTION
The samples were taken from a mine located in Shanxi Province, western China. Block coal, block mix (coal that has high percentage of ash or rock content) and block rock were sheared to square shapes. Each sample had the same surface area and thickness "10cm $\times$ 10 cm $\times$ 5cm", as seen in Fig. 3. The gray rock in Fig. 3-d was coated by a thin layer of coal powder or "coal dust" in order to add it as a fourth experimental sample; see Fig. 3-c. The chemical analysis was conducted for four samples to estimate the percentage of the components of each sample, such as moister (Mad), ash (Aad), volatile matter (Vad) and fixed carbon content (FCad); the results are shown in Table 1.

TABLE 1. Component of samples per gram.

No.	Name	Mad%	Aad%	Vad%	FCad%
a	Coal	5.82	2.99	35.44	55.75
b	Mix	5.40	22.44	38.27	33.89
c	Black rock	0.63	90.17	7.60	1.61
d	Gray rock	0.63	90.22	7.58	1.57

Moreover, other coals and gangues were randomly collected from the same mine. The random samples have different areas, size, thicknesses, shapes and surface conditions.

B. INFRARED RADIATION PRINCIPLE

The infrared radiation (IR) of an object is emitted above absolute zero due to the vibrations of atoms and molecules [14]. The vibrations of atoms increase with the increasing temperature of the object surface [14]. There are instruments that can sense the IR, such as passive infrared sensors and active infrared sensors [15]. The differences between two is the operating principle; for instance, the first detects IR based on thermal radiation that is radiating from an object, whereas the second receives the reflected IR that it essentially radiated toward an object [15]–[17]. The work in this paper is based on a passive infrared sensor. The emissivity, area, temperature and surface condition of the object are factors that impact the infrared radiation energy [14], [18].

The emissivity is the ratio of the real radiation energy emitted to the theoretical radiation energy emitted, which is called blackbody [14], [18], [19]. In addition, the emissivity is a dimensionless number between zero, "reflecting all radiation energy", and one, "emitting all radiation energy". For a blackbody, the emissivity equals one [14]. The emissivity is an unstable factor in thermal radiation energy, since it changes with temperature, wavelength as well as surface condition [14].

There are differences in both components besides properties of coal and rock, as shown in Table 1. These differences make the emissivity vary [14]. From this point, we can analyze the image that appears in the IC, thereby effectively determining whether it is coal or gangue depend on the radiation energy emitted, which is expressed as follows:

$$G_b = \frac{\partial \varphi}{\partial A} = \varepsilon \sigma T^4 \tag{1}$$

$$\varphi = \frac{\partial Q}{\partial t} \tag{2}$$

$$Q = h\delta = h\frac{c_0}{\lambda} \tag{3}$$

where ε is the emissivity, and $\sigma = 5.67 \times 10.8$ W/m^2. K is the Stefan–Boltzmann constant, and T is the surface temperature of the object. G_b is the total emissive power, $h = 6.62607015 \times 10^{-34}$ J · s is Planck's constant, δ is the frequency of the electromagnetic wave, λ is the wavelength, c_0 is the speed of light, and Q is the radiant energy or photon energy [12], [14], [20]. The total hemispherical emissivity can
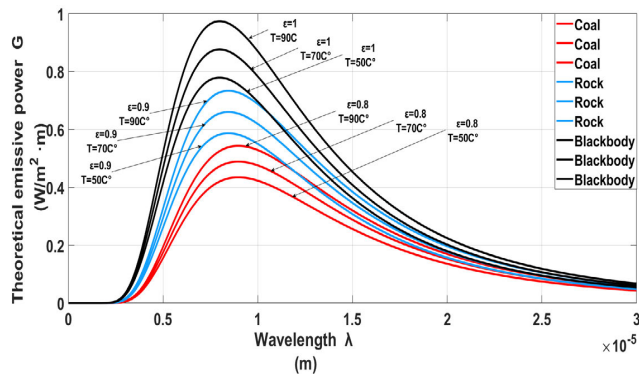
FIGURE 4. Comparison between blackbody, coal and rock emissive power with wavelength at different temperatures [14].

be obtained from equation (4):

$$\varepsilon = \int_0^\infty \frac{\varepsilon_\lambda G_{r\lambda}(\lambda, T)}{\sigma T} d\lambda \tag{4}$$

Approximately, we can obtain

$$G = \varepsilon \frac{c_1}{\lambda^5 \left[\exp\left(\frac{c_2}{\lambda T}\right) - 1\right]} \tag{5}$$

where G is a theoretical emissive power. The total emissive power can be obtained as

$$G_b = \varepsilon \int_0^\infty \frac{c_1}{\lambda^5 \left[\exp\left(\frac{c_2}{\lambda T}\right) - 1\right]} d\lambda = \varepsilon \sigma T^4 \tag{6}$$

where

$$c_1 = 2\pi h c_0^2 = 3.742 \times 10^8$$
$$c_2 = h c_0/k = 1.439 \times 10^4$$

Fig. 4 illustrates the effect of the changes in the surface temperature of the sample, whereas the emissivity of the sample is constant [14]. Fig. 4 also displays the impact of the changes in the emissivity of the sample, whereas the surface temperature is steady, on the emissive power of the sample [14]. Theoretically, separation between coal and gangue based only on the emissivity factor at constant temperature is possible.

C. INSTRUMENTATION AND STEPS

1) INFRARED IMAGE ACQUISITION

This laboratory trial and analysis were conducted on coal, mix, black rock and gray rock samples in order to distinguish between them in a simulated environment. The thermography acquisition setup composed of an IC (Ti32, FLUKE, Washington, USA, resolution: 320×240, sensitivity: 0.05°C, ccuracy: ±2 %, spectral band: 8 μm to 14 μm, sensor type: uncooled microbolometer, range: −20°C to 600°C), heater (LICHEN), base board and personal computer (PC). The base board was made of Teflon to minimize light reflection. The heater was used to provide thermal energy and evenly

FIGURE 5. Infrared image acquisition device.

FIGURE 6. The automated coal–gangue separation system with computer vision. PLC: Programmable Logic Controller, heating unit, IC and manipulator [3], [16], [17], [21].

FIGURE 7. Digital image acquisition device.

distributed the heat on the surface of samples between 50°C and 90°C. The IC was mounted over the base board for capturing the sample image, as displayed in Fig. 5.

The procedures of the laboratory trial were divided into two separate stages:

- The coal-rock images were directly captured at temperatures of 50°C, 70°C and 90°C after they had been heated by the heater. The coal, mix and rocks samples have the same area with a smooth surface. The image acquisition setup was carried out in a dark environment.
- Likewise, the laboratory trial was performed using coal and gangue samples that had different areas at temperatures of 50°C, 70°C and 90°C and under diverse illumination conditions.

First, the samples were placed in the heater to equally gain thermal energy. Once the furnace had heated the samples, the infrared images were immediately captured. The infrared images that were taken by the IC were sent to the PC to analyze them and study the rate of change in the histogram for each image with increasing temperature. According to the difference emissivity of the materials, the images appeared disparate. Furthermore, the variation in the image can be easily identified for samples that have different areas; nevertheless, the samples should be at the same temperature. Based on this point and heat transfer laws that are compatible with this investigation, we observed that it is feasible to separate gangue from coal by utilizing this technique. Fig. 6 demonstrates the steps and the aim of the proposed method.

2) DIGITAL IMAGE ACQUISITION
The main purpose of this experiment is to perform a comparison between digital and infrared images in order to illustrate and demonstrate the drawbacks of machine learning that utilized an industrial digital camera in the field of coal
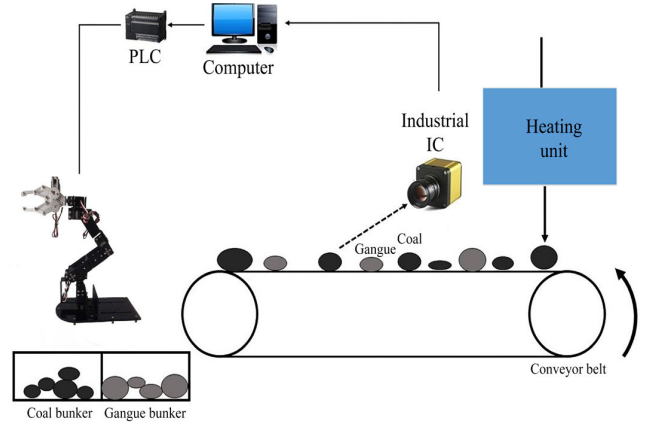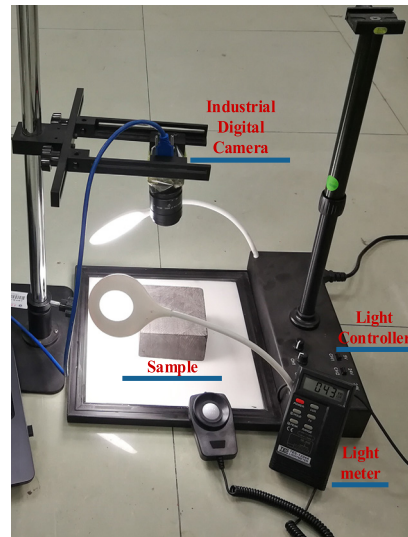
and gangue classification. Briefly, we prove why the discrimination system using a digital camera is inefficient in mining factories. As displayed in Fig. 7, the digital acquisition setup consists of an industrial digital camera (MER-230-168U3M, GET CAMERAS, Eindhoven, Netherlands, resolution: 1920 × 1200, sensor type: IMX174, pixel size: 5.86 μm), light meter (TES-1334A, TES, Taipei, Taiwan, sensitivity: 0.01 lux, accuracy: ±3 % rdg ±0.5 %, range: 0 to 20,000 lux/fc) to measure the intensity of visible light, light-emitting diode (LED) to provide suitable light and light controller to control the intensity of light.

In the first step, we put the sample perpendicular to the camera. Then, the first image is captured at a specific intensity of light; thereafter, the intensity of light was gradually changed. At each change, we recorded the value of intensity of light by using the light meter and captured photos at the same time. Then, the data were collected to analyze the relationship between the texture features of the digital image

with the changing light intensity because the light is a critical parameter in machine learning, particularly in discrimination systems to distinguish between coal and gangue.

D. FEATURE EXTRACTION OF COAL AND GANGUE

In general, the image has statistical features and visual features. Brightness, color and shape represent visual features [7], [12]. Statistical features are divided into two types based on gray level information (GLI) and grey-level cooccurrence matrix (GLCM) [10], [12]. The feature extraction depending on GLCM is more reliable than GLI in ordinary images [2], [9] because the gray level and its mean value are irregular, particularly for coal and rock images [2]. Moreover, there is no relation between feature extraction based on the GLCM and the mean value of gray [2]; as a result, this method is chosen in addition to GLI in this paper to inspect the practical applicability for infrared images.

1) FEATURE EXTRACTION BASED ON GLI

MATLAB 2019a was used to accomplish all this work. Before extraction, the RGB picture was converted into a gray picture using this formula:

$$J = 0.299R + 0.587G + 0.114B \qquad (7)$$

Then, the average intensity F_1 and average contrast F_2 were determined as follows [12]:

$$F_1 = \sum_{i=0}^{255} l_i J(l_i) \qquad (8)$$

$$F_2 = \sqrt{\psi_2} \qquad (9)$$

$$\psi_2 = \sum_{i=0}^{255} (l_i - F_1)^2 J(l_i) \qquad (10)$$

where l is a random variable indicating intensity, there are $J(l_i)$ intensity histogram levels in a region, and ψ_2 is the standard division [12].

2) FEATURE EXTRACTION BASED ON GLCM

The GLCM (U) is estimated as follows:

Assuming $J(x, y)$ is a *2D* image, H is the set of two pixels, which have correlation within the target area S [12].

$$U(i_1, i_2) = \#\{[(x_1, y_1), (x_2, y_2) \in H|(x_2, y_2)] = i_2\} \qquad (11)$$

where i_1, i_2 are pixel values. $U(i_1, i_2)$ denotes the numbers of each of the two pixels, which pixel values correspond to i_1 and i_2 in the region **R**. # is the number of pixels. Image normalization is performed to make them obey a normal distribution:

$$U_N(i_1, i_2) = \frac{U(i_1, i_2)}{N} \qquad (12)$$

After creating the GLCM image, we compute feature extraction textures, which are contrast F_3, energy F_4,

homogeneity F_5 and entropy F_6, as follows

$$F_3 = \sum_{i=1}^{D} \sum_{j=1}^{D} (i-j)^2 U_N(i,j) \qquad (13)$$

$$F_4 = \sum_{i=1}^{D} \sum_{j=1}^{D} U_N(i, j)^2 \qquad (14)$$

$$F_5 = \sum_{i=1}^{D} \sum_{j=1}^{D} \frac{U_N(i, j)}{1 + |i - j|} \qquad (15)$$

$$F_6 = -\sum_{i=1}^{D} \sum_{j=1}^{D} U_N(i, j) \log U_N(i, j) \qquad (16)$$

3) COLOR EXTRACTION BASED ON YCbCr

Feature extraction based on both GLCM and GLI are technically inconsistent when the difference areas, sizes, and surface conditions of the coal and gangue samples have been applied on classifier function, after computing the value of texture feature for each infrared image. Therefore, the YCbCr color space is presented in this paper to improve the accuracy of classification and decrease the time complexity, since only one feature is used in the classification system. The extraction feature from both GLCM and GLI are stable in one case, whereas the areas, sizes and surface conditions are similar. In this case, we can obtain acceptable results. Nonetheless, it is practically impossible in realistic working conditions to make whole block coal and block gangue have the same physical and geometric properties.

YCbCr is a digital color system; it is one kind of color space that is used in digital video [22], [23]. This kind of family space can be elicited from RGB by using the following transformation matrix:

$$\begin{bmatrix} Y \\ Cb \\ Cr \end{bmatrix} = \begin{bmatrix} 16 \\ 128 \\ 128 \end{bmatrix} + \begin{bmatrix} 0.257 & 0.504 & 0.098 \\ -0.148 & -0.291 & 0.439 \\ 0.439 & -0.368 & -0.071 \end{bmatrix} \begin{bmatrix} R \\ G \\ B \end{bmatrix} \qquad (17)$$

YCbCr comprises a luminance component, which is expressed by Y, and chrominance factors, which are described by Cb and Cr. Y - brightness (luma), Cb - blue1 minus luma and Cr - red minus luma [23].

Having heated and captured infrared images for coal and gangue samples, we sent them to the PC for image processing; thereafter, the infrared images were converted from the RGB to YCbCr color space, and then the Cb was isolated for whole coal and gangue images as

$$Cb = 128 - 0.148R - 0.291G + 0.439B \qquad (18)$$

After converting the images to the YCbCr color space and isolating the Cb canal, image segmentation is performed to generate a binary image BW. A threshold value is used to perform image segmentation, which separates the color from $(7, 131, 0)$ to $(254, 252, 0)$ RGB, which tends to be yellow in coal RGB images as background, and the remaining pixel are
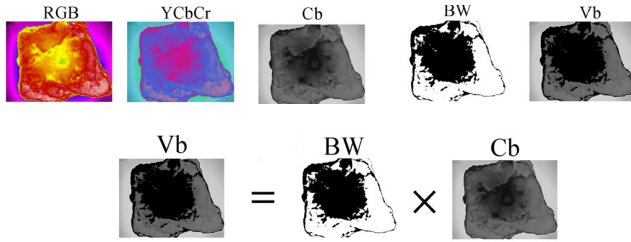
FIGURE 8. Steps of image segmentation.

considered to be the foreground. We used color thresholder app in MATLAB in order to manually determine the threshold value. Let *Cb* denote $Cb(x, y)$, a *2D* image:

$$BW = \begin{cases} 1 & \text{if} & Cb(x, y) > C_{bext} \\ 0 & \text{if} & Cb(x, y) \leq C_{bext} \end{cases} \quad (19)$$

where $C_{bext} = 88$ is the threshold value, and $Cb(x, y)$ is pixel value at x row and y column of the image *Cb*. After extracting the specific color from the coal images, the coal and gangue images are converted from binary images *BW* into *Vb* images by using the command "$Vb = \text{uint8}(BW)$. $*Cb$" in MATLAB. It should be noted that the binary image *BW* is a matrix that has a known number of x rows and y columns. The pixel values of this image are zero or one, and we need to convert the cell in the matrix of the binary image into unsigned integers of 8 bits (uint8) to contain all the numbers from 0 to 255. Then, we multiply it by the original *Cb* matrix to produce a new matrix called *Vb*. Fig. 8 illustrates the stages of image processing of the RGB infrared image and shows the segmentation process for obtaining the *Vb* image, which is the result of matrix multiplication of *BW* with *Cb* to produce a new matrix known as the matrix product *Vb*:

$$Vb = BW \cdot Cb \quad (20)$$

Then, the mean value of the *Vb* matrix is determined by this formula:

$$x_i = \frac{\sum \varpi_b}{p_b} \quad (21)$$

where x_i is the mean value of *Vb*, $i = 1, 2, \ldots, n$, ϖ_b is the pixel value in each x row and y column of *Vb* matrix, p_b is the total number of pixels, and n is the number of images. Subsequently, x_i is imported into the SVM for discriminating whether the x_i belong to coal or gangue, as presented in Fig. 9.

E. SUPPORT VECTOR MACHINE (SVM)

SVM is a mathematical algorithm applied in machine learning [24]. Additionally, SVM is commonly used in image recognition because it is the most effective among other types of classifiers [25]–[27]. SVM has been suggested as the classifier in this paper because it has high accuracy, and it is suitable for small data [8], [10], [28]. Moreover, SVM can handle certain cases, such as nonlinearity, by using nonlinear basis functions or kernel functions. SVM also has a powerful method to prevent overfitting [25], [26], [28]. The most
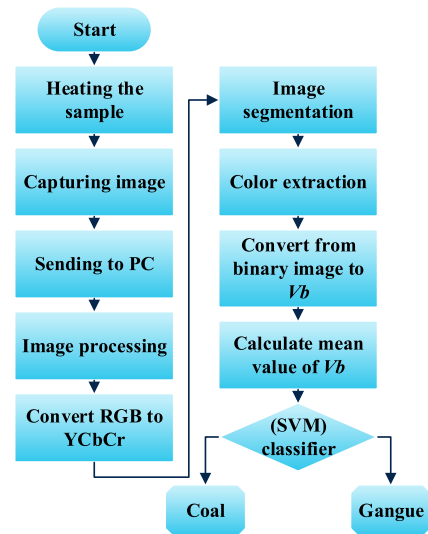

FIGURE 9. Schema for the purpose of the system.

important advantage of SVM is that it can work with a large number of features without incurring great computational complexity [25]–[29].

The decision rule of SVM is the following [30]:

$$\begin{aligned} g(x_1) &= w^T x_1 + b > 0 & \rightarrow & \quad x_1 \in Gangue \\ g(x_1) &= w^T x_1 + b < 0 & \rightarrow & \quad x_1 \in Coal \end{aligned} \quad (22)$$

where x_1 is a specific point unknown vector in plan $\mathbf{R}^2$. Consider a sample set $M = (x_i, y_i)$, $i = 1, 2, \ldots, n$, x_i is the input date points, where $x_i \in \mathbf{R}^d$, y_i is the output label $y_i \in (1, -1)$, and n is the number of training samples [27]. They are separated by a decision surface given by $\mathbf{w}^T \mathbf{x} + b = 0$, where $\mathbf{w}$ is a d-dimensional coefficient vector that is normal to the decision surface and is called a hyperplane, and b is the distance of the decision surface from the origin [27]. The optimal separating margin can be obtained by solving the following optimization problem:

$$\text{Min } g(\mathbf{w}, \xi) = \frac{1}{2}||\mathbf{w}||^2 + C \sum_{i=1}^{n} \xi_i$$

$$s.t., \quad y_i(\mathbf{w}^T \mathbf{x}_i + b) \geq 1 - \xi_i, \quad \xi_i \geq 0 \quad (23)$$

C denotes the distance of error points to their correct zones, and ξ_i denotes a slack variable.

There are many cases in which the data points in feature space cannot be linearly separated [27]. To make SVM more effective in nonlinear feature spaces [27], [30], the original input data in plan $\mathbf{R}^2$ are mapped into higher-dimensional feature space $\mathbf{R}^d$ where the data set are linearly separable, $g: \mathbf{x} \rightarrow \phi(\mathbf{x})$ [27]. We know that the linear classifier depends on the dot product $K(\mathbf{x}_i, \mathbf{x}) = \mathbf{x}_i \cdot \mathbf{x} = \mathbf{x}_i^T \mathbf{x}$. Then, the dot product becomes

$$K(\mathbf{x}_i, \mathbf{x}) = \phi(\mathbf{x}_i)^T \phi(\mathbf{x}) \quad (24)$$

TABLE 2. The common kernel functions.

Kernel types	Kernel functions	Hyperparameters
Linear kernel	$K(x, x_i) = x^T x_i$	C and $\gamma > 0$
Polynomial kernel	$K(x, x_i) = (\gamma(x^T x_i) + 1)^u$	C, u and $\gamma > 0$
Gaussian kernel (RBF)	$K(x, x_i) = \exp(-\gamma \|x - x_i\|^2)$	C and $\gamma > 0$
Cubic kernel	$K(x, x_i) = (x^T x_i)^3$	C and $\gamma > 0$

Therefore, hyperplane function can be expressed as

$$g(\mathbf{x}) = \text{sgn}\left(\sum_{i=1}^{n} \alpha_i y_i K(\mathbf{x}_i, \mathbf{x}) + b\right) \qquad (25)$$

There are many types of kernel functions, as presented in Table 2. The polynomial and Gaussian (Radial-based kernel RBF) are common kernels among other types in SVM [27]. The functions of these kernels are also listed in Table 2, where γ is parameter kernel that controlling the width of the kernel [27], and u is the polynomial order [27]. To build a reliable classification model, the hyperparameters C, γ and u must be optimized because the best parameter values ensure the minimum classification error [28], [29]; consequently, the best performance of SVM can be obtained [25]–[27]. In this study, the values of hyperparameters C and γ were tuned by using Bayesian optimization; then, the hyperparameters value were applied in the classification learner app in MATLAB.

IV. TIME ANALYSIS AND METHODOLOGY DESIGN

This section discusses the required time "time complexity" to accomplish the process from the beginning of the sample entry to heating unite until the termination process "SVM classifier". In this section, we also elaborate and analyze the parameters that influence the time complexity. To simplify the analysis and time complexity calculation, this methodology should be divided to three critical processes (heating process, image reading-processing and classification process), as presented in Fig. 10. Every single process includes parameters that affect the time and performance of the methodology. We study and analyze each parameter that influences the time complexity.

A. TIME ANALYSIS OF HEATING PROCESS

The time of infrared image acquisition depends upon the required time that the object needs to reach the desired temperature. However, it is difficult to accurately evaluate the required time, since we are studying the physical phenomenon. Before studying the time complexity, some basics of heat transfer should be elaborated. The heat transfer from one specific point to another point occurs by conduction in solids, convection in fluids and radiation in spaces or gases [14], [20]. Additionally, when heat transfers from point to point, it travels in 3-dimensional space [14], [20]. In our case, the heat transfer from heating unit into the samples or
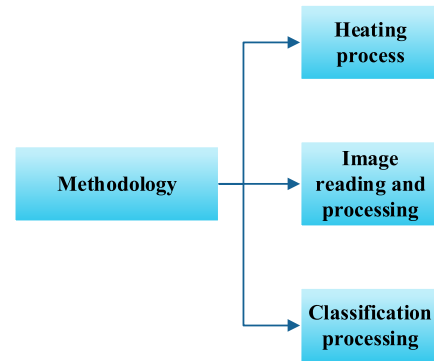

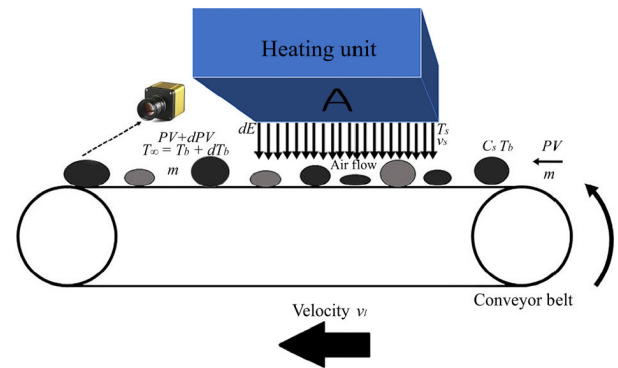**FIGURE 10.** Methodology analysis for computing time complexity.

FIGURE 11. Thermal analysis for heating process.

object is due to convection, as shown in Fig. 11. The conveyor fluid that carries the heat energy from the heating unit toward the samples is air. The convection is divided into two types, forced convection, "when an external machine is used to pump the fluid", and natural convection, "no machine is used to move the fluid" [14]. Furthermore, there are parameters and factors that impact the heat transfer [14], [20], e.g., the physical properties of the samples, the physical properties of the conveyor fluid and the specifications of the heating unit, as displayed in Fig. 11.

To estimate the required time of heating process "infrared image acquisition", the law of conservation of energy [14], [20], which states that the total energy that enters the system equals the total energy that exits the system, is applied at steady state temperature $\frac{\partial T}{\partial t} = 0$ and one-dimensional heat transfer [14], [20], as shown in Fig. 11

$$dE + \frac{\partial m}{\partial t} c_{pm} T_b + \frac{\partial m}{\partial t} PV = \frac{\partial m}{\partial t} c_{pm} T_\infty + \frac{\partial m}{\partial t}(PV + d(PV)) \qquad (26)$$

$$c_{pm} = \frac{C_s}{m} \qquad (27)$$

$$C_s = \lim_{\Delta T \to 0} \frac{\Delta q}{\Delta T} \qquad (28)$$

Because the system is incompressible, $PV = 0$, where P is pressure, V is volume and q represents the heat energy. The

required time can be expressed as

$$dt_{heat} = \frac{c_{pm}m(T_\infty - T_b)}{dE} \tag{29}$$

where c_{pm} is the specific heat capacity of sample, m is the mass of sample, and T_b and T_∞ are the surface temperatures of the object before and after heating process, respectively. The heat capacity C_s is a physical property that changes with the change in matter; it is the required heat energy q that must be added to the object to increase its temperature by one degree Celsius. E represents the heat added that transfers from the source of thermal energy "heating unit" to the object by forced convection, which is expressed as

$$dE = hA(T_s - T_b) \tag{30}$$

where h is the convection heat transfer coefficient, A is the area of the heating unit, and T_s is the temperature of the heating unit surface.

$$h = \frac{Nu\,k}{L_c} \tag{31}$$

We notice in equation (31) that the convection heat transfer is proportional to the Nusselt number Nu and thermal conductivity k of the fluid "air" that transfers the heat from the heating unit to the sample. Furthermore, the convection heat transfer is inversely proportional to the length L_c of the sample or object that we want to heat it. The Nusselt number is a dimensionless number; for a given geometry, it can be expressed in term of the Reynolds and Prandtl numbers as

$$Nu = B\,Re^\kappa\,Pr^\varsigma \tag{32}$$

where B is a constant that depends on the geometry of the object, Re is the Reynolds number and Pr is the Prandtl number. κ and ς are also constants that depend on the value of the Reynolds number, which are estimated as

$$Re = \frac{\rho v L_c}{\mu} \tag{33}$$

$$v = \sqrt{v_l^2 + v_s^2} \tag{34}$$

where v is the magnitude of the belt velocity v_l in the x direction and air velocity v_s in the y direction, as shown in Fig. 12. ρ and μ are the density and viscosity of air, respectively,. After calculating the Reynolds number, the Nusselt number can be estimated over flat plate as

$$\text{Laminar: } Nu = 0.664Re^{0.5}Pr^{1/3}$$
$$Re < 5 \times 10^5, \quad Pr > 0.6 \tag{35}$$
$$\text{Turbulent: } Nu = 0.037Re^{0.8}Pr^{1/3}$$
$$5 \times 10^5 \leq Re \leq 10^7, \quad 0.6 \leq Pr \leq 60 \tag{36}$$
$$Pr = \frac{\mu c_{pf}}{k} \tag{37}$$

where the Prandtl number Pr is the ratio of the molecular diffusivity of momentum to the molecular diffusivity of heat [14], and c_{pf} is the specific heat capacity of the air. If we assume that the pressure of air is constant
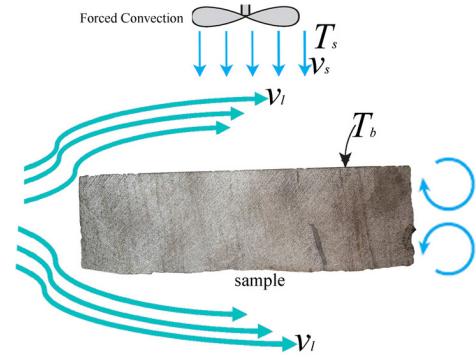

FIGURE 12. Schema for velocity analysis and air dynamics over the sample [14].

$\frac{\partial P}{\partial x} = 0, \quad \frac{\partial P}{\partial y} = 0$ [14], the air properties (ρ, μ, k, c_{pf}) can be obtained from tables in [14].

Equations (35) and (36) were selected because the geometry of majority of random samples in this study are near the flat plate. The Reynolds and Prandtl numbers are dimensionless quantities. Based on the value of Reynolds number, we can determine whether the fluid is laminar or turbulent. It can be observed in equation (33) that the velocity v is proportional to the Reynolds number Re. Therefore, the value of the Nusselt number Nu will be large. It should be noted that the large Nusselt number enhances the convection heat transfer coefficient h. Thus, we can obtain the prefect heat transfer; however, a high value of velocity v leads to low heat transfer practically [14].

Therefore,

$$t_{heat} = \frac{c_{pm}mL_c(T_\infty - T_b)}{B\left(\frac{\rho v L_c}{\mu}\right)^\kappa \left(\frac{\mu c_{pf}}{k}\right)^\varsigma kA(T_s - T_b)} \tag{38}$$

where t_{heat} denotes the time of infrared image acquisition. The heating unit should be designed depending on the largest expected volume and density of the sample that came from the colliery. Here, the largest volume and density should be considered in the heating process, as they are proportional to the time of infrared image acquisition. To clarify, when the volume of the sample is large, it needs more thermal energy in order reach the desired temperature T_∞; consequently, a large sample requires more time to heat up than a small sample. The mass of sample can be obtained as

$$m = \rho_{sam}V_{sam} \tag{39}$$

where ρ_{sam} denotes the density of sample, and V_{sam} denotes the volume of the sample; however, in this system, we need to heat the surface area of the sample, not the whole volume of the sample, since the infrared radiation that we need to collect in order to discriminate between coal and gangue depends on the surface area of the sample [14]. Note that, the radiation emitted by the interior regions can never reach the surface [14]. Therefore, we can neglect the depth of sample and then calculate only the largest expected area of the sample that will come from the colliery. Thus, the mass

area of sample can be written as

$$\bar{m} = \rho_{sam} A_{sam} \tag{40}$$

substituting equation (40) into equation (38) yields

$$t_{heat} = \frac{c_{pm}\rho_{sam}A_{sam}L_c(T_\infty - T_b)}{B\left(\frac{\rho v L_c}{\mu}\right)^\kappa \left(\frac{\mu c_{pf}}{k}\right)^\varsigma kA(T_s - T_b)} \tag{41}$$

All the parameters presented in Table 3 can be controlled except for the mass of the samples that randomly come from the colliery with different sizes, lengths, densities and shapes. Equation (41) can be simplified as

$$t_{heat} = CTP \times \frac{c_{pm}\rho_{sam}A_{sam}L_c}{B} \tag{42}$$

where

$$\rho_{sam} = \frac{1}{((1 - a - w_w)\rho_o^{-1}) + (a\rho_a^{-1}) + (w_w\rho_w^{-1})} \tag{43}$$

$$c_{pm} = (1 - a - w_w)c_o + ac_a + w_wc_w \tag{44}$$

$$c_a = 752 + 0.293T_{avg} \tag{45}$$

$$T_{avg} = \frac{T_s + T_b}{2} \tag{46}$$

where CTP denotes the value of the controlled thermal parameters, ρ_o, ρ_a and ρ_w represent organic fraction, ash and water densities, c_o, c_a and c_w denote the specific heat capacity of organic fraction, ash and water, respectively. "a and w_w" represent weight percentage of ash and water content of sample, respectively [31], T_{avg} is average temperature. The specific heat capacity, density, area, and length of the sample, c_{pm}, ρ_{sam}, A_{sam} and L_c, respectively, are critical parameters in the heating process; however, these critical parameters can be overcome by calculating the maximum expected specific heat capacity, density, area as well as length of the sample. Note that the maximum size and length of the coal and gangue block can be controlled by the shearer and equipment associated with it in coal mine. The maximum value of critical parameters should be considered in order to ensure the small samples exit from the heating unite at same temperature of large samples. Shortly, the heat energy and time that consume to raise the temperature of small sample is much less than larger sample.

The volatile matter are produced during combustion of organic matter in sample at 900° C; however in heating process the temperature of samples are 50°C, as a result the weight percentage of organic fraction equal sum of weight percentage of volatile matter (Vad) and fixed carbon content (FCad).

Table 3 summarizes all the physical complexity parameters with their values that influence the infrared image acquisition time, which is essentially directly associated with time of heating process.

B. TIME ANALYSIS OF IMAGE READING, PROCESSING AND CLASSIFICATION

The time complexity was determined by attracting the code. The time complexity of image processing depends on the

TABLE 3. The values of physical parameters.

Symbol	Quantity	Value
ρ	density of air flow	$1.1092\,\text{kg/m}^3$
c_{pf}	specific heat capacity of air flow	$1.007\,\text{kJ/kg}\cdot\text{K}$
μ	viscosity of air flow	$1.963\times10^{-5}\,\text{kg/m}\cdot\text{s}$
k	thermal conductivity of air flow	$0.02735\,\text{W/m}\cdot\text{K}$
κ	constant	0.5
ς	constant	0.8
A	area of heating unit	$7\,\text{m} \times 1\text{m}$
T_s	temperature of heating unit	70°C
T_b	surface temperature of sample before the heating	30°C
T_∞	surface temperature of sample after the heating	50°C
A_{sam}	surface area of sample	$0.0625\,\text{m}^2$
L_c	length of sample	0.3 m
B	geometry factor	0.66
ρ_o	density of organic fraction	$1250\,\text{kg/m}^3$
ρ_a	density of ash	$2555\,\text{kg/m}^3$
ρ_w	density of water	$990.2\,\text{kg/m}^3$
c_o	specific heat capacity of organic fraction	$1.134\,\text{kJ/kg}\cdot\text{K}$
c_a	specific heat capacity of ash	$0.76665\,\text{kJ/kg.K}$
c_w	specific heat capacity of water	$4.181\,\text{kJ/kg}\cdot\text{K}$
a	weight parentage of ash	0.0299
w_w	weight parentage of water	0.0582
v_l	velocity of conveyor belt	0.872 m/s
v_s	velocity of air	1.8 m/s

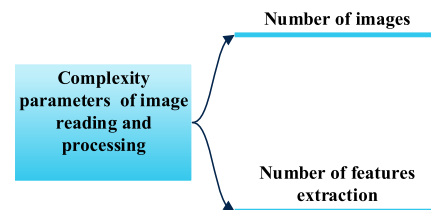Air and water properties at T_{avg}= 50°C and $P = 101325$ N/m^2

FIGURE 13. Complexity parameters of infrared image reading and processing.

number of images (n) and number of features extracted (F), as displayed in Fig. 13. Note that the image is a matrix. This matrix mainly has (r) rows and (p) columns. Therefore, the time complexity of image reading and processing is $O(\text{reading-processing}) = O(n*F*r*p^2)$.

In the case of the classification process shown in Fig. 14, the time complexity of the training process depends on the number of training samples (x_i) and the number of features $O(x_i^2*F^2)$. Moreover, the time complexity of the prediction process depends on the number of support vectors (s_v), which depends on the number of testing sample ($\dot{x}_i$); it also depends on the number of features $O(\dot{x}_i *s_v*F)$. Therefore, the total time complexity of the classification process is $O(\text{SVM}) = O(x_i^2*F^2) + O(\dot{x}_i*s_v*F)$.

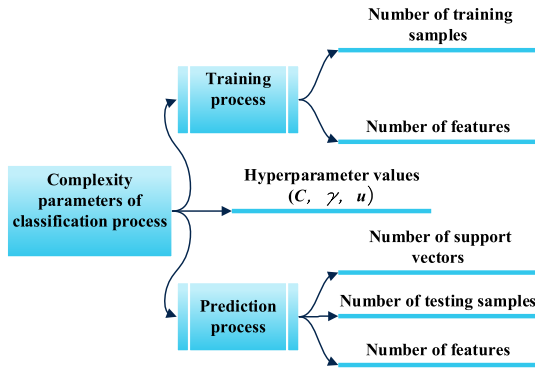The overall time complexity of acquisition, reading, processing, training and prediction of infrared image can be

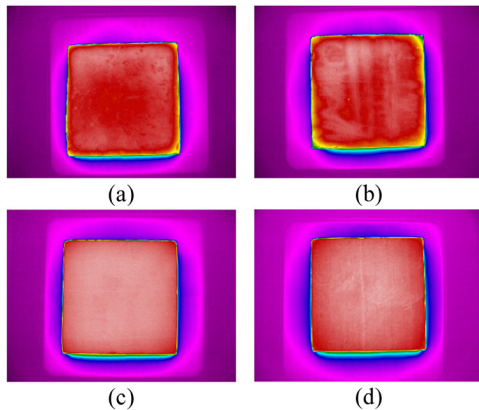**FIGURE 14.** Complexity parameters of classification process.

FIGURE 16. Infrared images at 70°C.

FIGURE 15. Infrared images at 50°C.

FIGURE 17. Infrared images at 90°C.

written as

$$T_{\text{total}} = t_{heat} + O(n\,F\,r\,p^2) + O(x_i^2 F^2) + O(\dot{x}_i s_v F) \quad (47)$$

It should be noted that the time of infrared image acquisition t_{heat} equals the time of heating process, at which time the maximum area of sample in the system consumes it to reach the desired temperature T_∞. At this moment, the infrared images were captured by the IC, and then, the time of image processing was evaluated. Next, the time of training process was calculated, and eventually, the time of the prediction process was estimated using a PC with Intel(R) Core (TM) i7-4810MQ CPU @ 2.8 GHz.

V. RESULTS AND DISCUSSION
A. RESULTS BASED ON GLI AND GLCM FEATURE EXTRACTION

As we mentioned in section III (see Fig. 4), there are correlations between the temperature, emissivity, wavelength and photons. We observe there are noticeable difference between coal and rocks in Fig. 15, Fig. 16 and Fig. 17. Regardless of the slight variations between coal and mix, the color tends to be yellow, can be seen in (Fig. 15-a), (Fig. 15-b), (Fig. 16-a), (Fig. 16-b), (Fig. 17-a) and (Fig. 17-b); it appears in all the co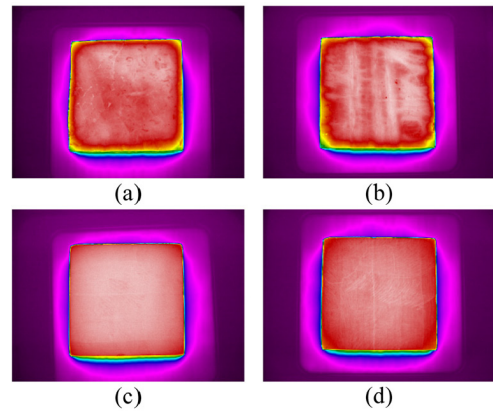al images, meaning that in samples that contain a high percentage of (FCad), we can notice this coloron them despite the temperature change.
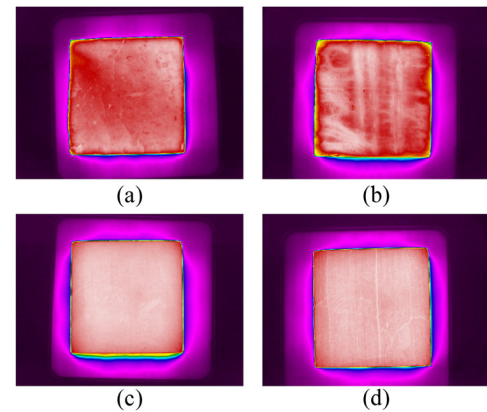
Although the gray rock (see Fig. 3-d) was coated by a thin layer of coal "grinded coal", the image is nearly the same as that of gray rock, as displayed in (Fig. 15-c), (Fig. 15-d), (Fig. 16-c), (Fig. 16-d), (Fig. 17-c) and (Fig. 17-d), which enables us to readily detect the rocks and then separate them. The slight variations that appear in the images between the coal and mix samples is due to the high percentage of rock in the mix sample. In addition, we can observe that the degree of red color clearly varies in Fig. 5, Fig. 16 and Fig. 17. Based on thermal radiation, this observation is logical because there is some discrepancy in the components between the coal and mix; therefore, the emissivity will be certainly disparate. At constant temperature, the difference in emissivity depends on the type of material and physical property; consequently, it directly influences the emitted thermal radiation and thus the photon energy is affected. Then, the differences between the images are deeply clear.

From Table 4, Table 5 and Table 6, we can observed that the energy, homogeneity and entropy are unstable compared with the average intensity and average contrast. There is also remarkable phenomenon in the average intensity; the value of the average intensity for coal is still lowest among

TABLE 4. Extraction features at 50°C.

Sample	Average intensity	Average contrast	Energy	Homogeneity	Entropy
Coal	76.8035	27.3357	0.0017	0.4448	10.0271
Mix	81.0857	30.5863	0.0031	0.5342	9.6689
Black rock	100.1075	43.8695	0.0023	0.5384	9.7481
Gray rock	96.5352	35.0536	0.0028	0.5427	9.7458

TABLE 5. Extraction features at 70°C.

Sample	Average intensity	Average contrast	Energy	Homogeneity	Entropy
Coal	76.1269	47.0486	0.0027	0.5610	10.0268
Mix	81.754	50.0325	0.0035	0.5781	9.9167
Black rock	90.724	58.0178	0.0027	0.6148	9.7290
Gray rock	80.4353	45.3022	0.0038	0.5996	9.6256

TABLE 6. Extraction features at 90°C.

Sample	Average intensity	Average contrast	Energy	Homogeneity	Entropy
Coal	71.7963	51.0129	0.0028	0.5266	10.1324
Mix	77.9655	55.5097	0.0030	0.4979	10.2810
Black rock	93.0598	73.2788	0.0042	0.5732	9.6208
Gray rock	94.475	72.6158	0.0029	0.5129	10.0236

the other samples despite a temperature change. Moreover, the value of the average contrast is still regular, implying that its value increases with temperature. As the emissivity of rock is higher than that of coal [14], since the percentage of ash content to fixed carbon content, moisture and volatile matter directly impacts the emissivity, thus the features extracted from the infrared images are certainly changeable.

A law was established by Max Planck in 1900, in conjunction with his *quantum theory*; this law is described in equations (1), (2), and (3), which state that photon energy is inversely proportional to wavelength, which is essentially inversely proportional to temperature. To clarify, when we increase the surface temperature of any object, the emitted radiation has a short wavelength: therefore, the photon energy becomes more active. This quantum theory clarifies the relationship between the increasing temperature and average contrast of an infrared image. If the temperature of the surface increases, the infrared image becomes clear, and the details of the image visibly appear.

B. RESULTS BASED ON COLOR EXTRACTION FROM THE YCbCr

This analysis was performed on 329 infrared images of coal and 271 infrared images of gangue at 50°C after conducting many tests involving GLI and GLCM features extraction besides RGB, HSV and L*a*b color spaces. The differences were clearly demonstrated in the YCbCr color spaces, predominantly in the blue minus luma *Cb*, as shown in Fig. 19. All the samples have different physical properties and surface conditions as displayed in Fig. 18, such as roughened or polished surfaces. Both Fig. 18 and Fig. 19 illustrate the main significant variation between coal and gangue.
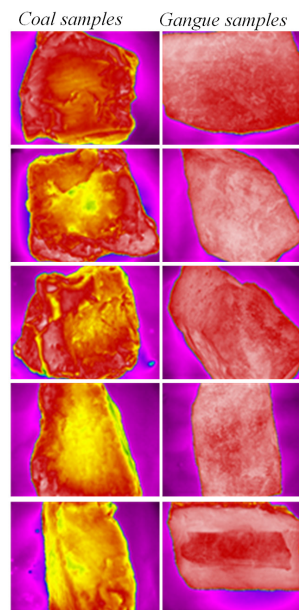
FIGURE 18. Infrared images for coal and gangue at 50°C with different area, size and surface conditions.
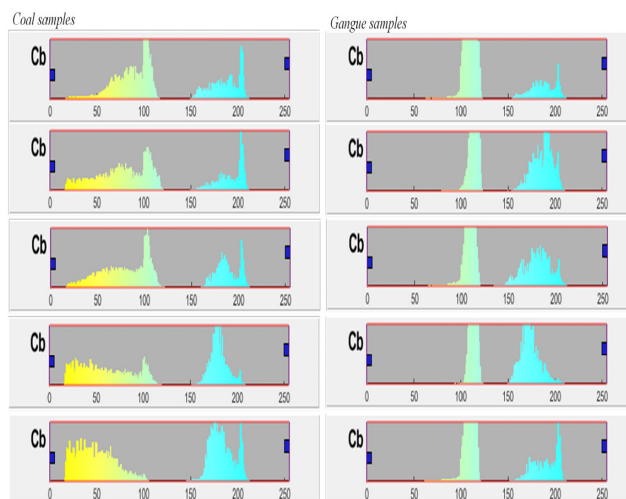
FIGURE 19. Histogram of blue minus luma Cb analysis for coal and gangue infrared images at 50°C.

Despite the diversity of the coal and gangue samples in terms of shape, size, area and surface condition, the main difference between coal and gangue is yellow color, which clearly appear in the whole coal samples, as shown in Fig. 19. We can also conclude from this experiment that the main difference between coal images and gangue images is the saturation of the yellow spectrum, which enable us to classify them effectively.

Fig. 20 and Fig. 21 show the distribution of the coal and gangue samples during the training. All the coal samples are in the accurate region except two samples, and all the gangue samples are in the exact region except only one; it lies in the common intersection between coal and gangue because some samples have mixed characteristic owing to

TABLE 7. The time results of acquisition, reading, processing, training and prediction of infrared images.

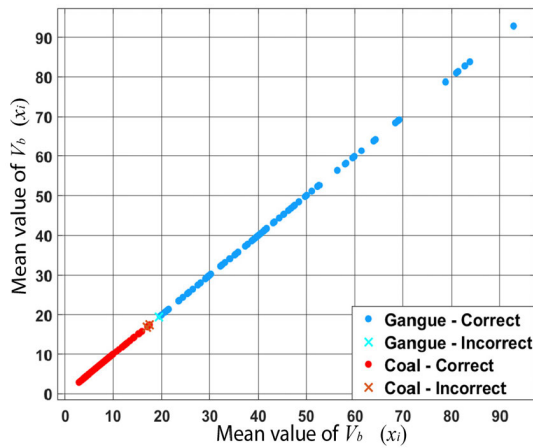| Algorithm	Training set	image Acquisition (s)	Image reading and Processing (s)	Training time (s)	Predication time (s)	Total time of system, T_{total} (s)
Linear SVM	200	855	5.8	0.89	0.00101	861.691
Polynomial SVM	200	855	5.8	1.179	0.00084	861.979
Gaussian SVM	200	855	5.8	1.169	0.00097	861.969
Cubic SVM	200	855	5.8	1.167	0.00078	861.967

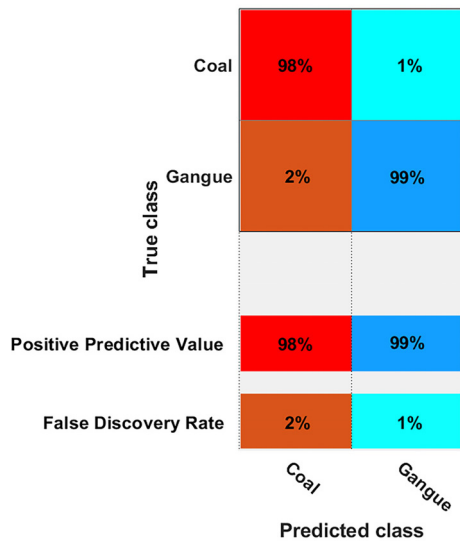**FIGURE 20.** The view of classification with Cb (Gaussian SVM).

FIGURE 21. Confusion matrix of training process (Gaussian SVM).

the percentage of rock content to fixed carbon content. From Fig. 20 it can be observed that the points of gangue have large values, whereas the coal points have small values in feature space because the emissivity of gangue is greater than that of coal [14]. As we discussed in section III, the photon energy is proportional to the surface temperature and the emissivity of an object (see Fig. 4). Deductively, Fig. 20 is compatible with *Max Planck's theory* and heat transfer laws, given by equations (1) (2), (3) and (6). When the emissivity increases

at constant temperature, the energy of the photons becomes more active; therefore, the mean value of $Vb (x_i)$ is large for state of the gangue in Fig. 20. Conversely, decreasing the emissivity at constant temperature causes the energy of the photons decrease; consequently, the mean value of $Vb (x_i)$ is small, as displayed in Fig. 20. We infer that the mean value of $Vb (x_i)$, equation (21), is proportional to the emissive power, equation (6).

Table 7 presents the results of acquisition, reading, processing and classification time of the infrared image; 200 original infrared images (100 for the coal samples and 100 for the gangue samples) were imported into the SVM classifier as training set. Note that the time of infrared image acquisition does not depend on the number of images. In other words, one image takes 855 s for heating in order to capture an infrared image for the sample at desired temperature T_∞; 200 images will take the same period of 855 s, 1000 images will also take 855 s, and so on because we calculated the time that the sample consumes from entering the heating unit until exiting it (see Fig. 11) and (see equation (41)). Once the sample exits the heating unit, we directly capture the infrared image using the IC. This time of heating is called the time of infrared image acquisition. We infer that the time of infrared image acquisition is independent of the number of samples.

Even though the environmental conditions of the experiment were not very accurate, e.g., the surface temperature of samples ranged from 51.5°C to 48°C, the background temperature was irregular, and the room temperature ranged between 26°C and 30°C, the classification test accuracy of the proposed method reached 97.83 % with only one selected feature, so the time complexity was substantially reduced. Keep in mind that the optimization process can lead to an overfitted model [13]. Therefore, before training, 229 samples of coal and 171 samples of gangue were isolated. The total number of original infrared images was 400 images, with 200 in the training set. Thus, the total number of original infrared images was 600 images. Then, we imported the images as the test set into the classification learner app. To extend our dataset and to ensure the performance and accuracy of the test set, we rotated the 600 images in three directions (i.e., by 180°, 270°, and 360°). Therefore, the infrared images become 2200 images used as the test set with different kernel functions as shown Table 8.

As demonstrated in Table 8, the test accuracy of Linear SVM is 96.66%, whereas stayed constant 96.66% in Cubic SVM with increasing in training time as shown in Table 7.

TABLE 8. The results of test samples.

Algorithm	Test set	C	γ	u	Error identification	Accuracy	Rotating test images	Accuracy
Linear SVM	600	0.001	0.008	N/A	20	96.66 %	2200	96.66 %
Polynomial SVM	600	0.001	0.008	2	16	97.33 %	2200	97.33 %
Gaussian SVM	600	10	4	N/A	13	97.83 %	2200	97.83 %
Cubic SVM	600	1	Auto	N/A	20	96.66 %	2200	96.66 %

There was a marked rise in the accuracy of Polynomial SVM reached 97.33% with rising in training time. Although the PC was old version (Intel(R) Core (TM) i7-4810MQ CPU @ 2.8 GHz), Gaussian SVM provided us high accuracy of training efficiently and rapidly, it attained 97.83% within 1.169s. We should consider not only the number of selected features influence on training time but the speed of processor also affects on time of training.

It is noticeable in Table 8 the accuracy fluctuations in different kernels due to the values of the hyperparameters (C, γ, u). To be specific, the accuracy and time of classification process depend on the hyperparameter values for the same kernel function with the number of images and number of features held constant. Note that increasing the parameter C led to minimizing the margin, and decreasing the parameter C yielded the maximum margin, as demonstrated in equation (23). Additionally, high values of parameter γ make the decision boundary wind around points in feature space. Conversely, reducing parameter γ results in a smooth decision boundary. Nevertheless, both decreasing and increasing the values of hyperparameters can minimize the error, depending on the form of the points vector in feature space.

The power of the proposed method is the stability of the accuracy when the 600 infrared images were rotated in three directions to extend the data set 2200 images, as provided in Table 8. The main reason for the accuracy stability is that the mean value of the Vb matrix (x_i) in equation (21) was estimated for each pixel of the whole infrared image. Consequently, when the infrared image is rotated, the value of the point vector in feature space never changes.

C. INFRARED IMAGE VERSUS DIGITAL IMAGE

The infrared image, digital image stability and the disadvantages of previous works are discussed in this section. As we mentioned in section II, the visible light is a critical parameter that affects the performance of the classifier because the industrial digital camera has a spectral band that ranges from 0.38 μm to 0.74 μm. Additionally, the multispectral camera has a spectral band from 0.665 μm to 0.975 μm; therefore, it is very sensitive to change in visible light intensity. Consequently, the points vector x_i in feature space will be changeable due to the external and internal factors that we mentioned in section II.

Thus, the performance of the classifier is low, i.e., "inefficient", or led to be is ineffectual due to disturbance of the point vector. Therefore, we infer that there are two important phenomena should be taken into consideration, namely,
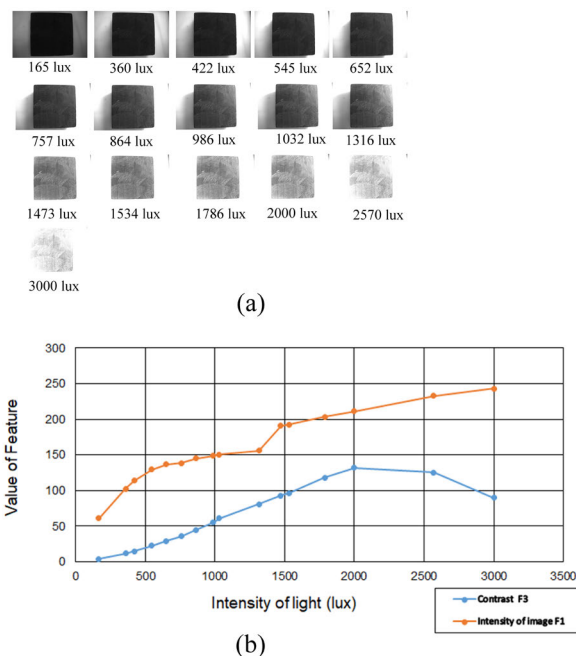

(a)

(b)

FIGURE 22. a- Analysis of ordinary images taken by the industrial digital camera (MER-230-168U3M, GET CAMERAS); b- the relationship between the contrast F_3 based on the GLCM and image intensity F_1 based on the GLI with change in the visible light intensity for same sample.

surface phenomenon [14] and **stability point vector phenomenon (SPVP)**.

The camera is a sensor that senses the electromagnetic waves that come from the sample, and then the electromagnetic wave "visible light or infrared radiation" are analyzed in order to determine whether the sample is coal or gangue. Here, the visible light or infrared radiation should pass through the "dust and haze" obstacles to reach the camera without losses to obtain correct information. **Surface phenomenon** refers to the ability of visible light or infrared radiation to pass the dust and haze to reach the camera. **SPVP** refers to the ability of the point vector in feature space to withstand changes in the external and internal factors. Conclusively, the **SPVP** has strong relation with surface phenomenon.To demonstrate this point, the experimental results of section III-*C* are presented in Fig. 22 and Fig. 23.

When the area, size, color and surface condition of the sample in Fig. 22-a are constant, the variation in the image intensity F_1 and contrast F_3 due to the variation in the visible light intensity are notable; thus, the point vector in feature space is changed, which will completely affect the performance of classifier, which used the industrial digital camera
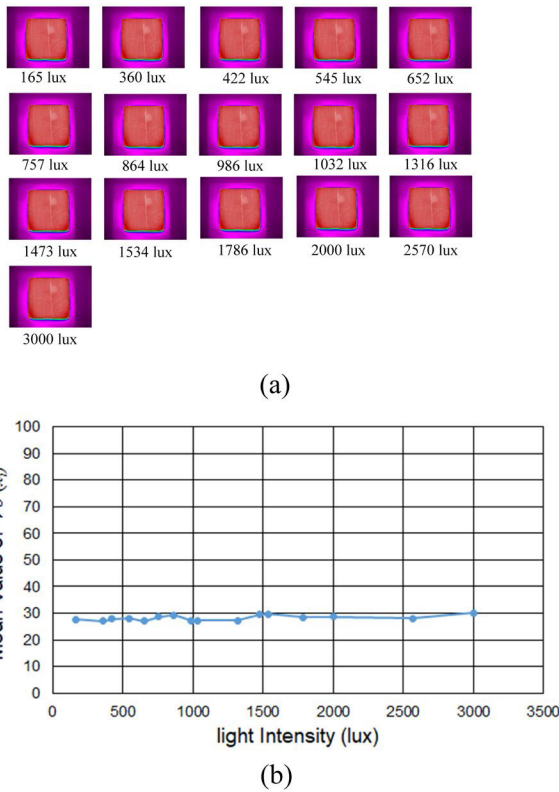
(a)

(b)

FIGURE 23. a- Analysis of infrared images taken by the IC (Ti32- FLUKE) at 50°C; b- the relationship between the mean value of Vb (x_i) with change in the visible light intensity at 50°C for same sample.

TABLE 9. Comparison of previous approaches.

Ref.	Authors	Type of camera	Method	Features	Accuracy
[5]	Yaqun *et al*	Digital	GA-ANN	GLI Mean variance. Skewness. Kurtosis. Energy. GLCM Angular second moment. Contrast. Inverse difference moments. Entropy.	100 %
[2]	Sun and Su	Digital	CID	GLCM Variance. Autocorrelation. Sum of variance. Sum of average.	94.12 %
[6]	Gao *et al*	Digital	RNRA	Value of gray scale.	96.8 %
[3]	Liu *et al*	Digital	KNN	GLI Average of the grayscale histogram. GLCM Second-order moment. MFDFA Geometric features.	97.5 %
[8]	Zhao	Digital	SVM	GLI Uniformity. Smoothness. Variance. Mean value. Three order matrix.	81 %
[9]	Sue *et al*	Digital	CNN	Extract features automatically based on GLI and GLCM.	95.88 %
[10]	Li and Sun	Digital	SVM	GLI Mean. Variance. Skewness. Peak. GLCM Contrast. Relevance. Entropy. Stability degree.	98.7 %
[4]	Hu *et al*	Multisp-ectral	SVM	Histogram of oriented gradient. Local binary pattern. Haar feature.	96.25 %

or multispectral camera. In other word, take two points from Fig. 22-b (e.g., at 360 lux $F_3 = 11.82$ and at 422 lux $F_3 = 14.73$), and subtract the two points from each other ($14.73 - 11.82 = 2.91$); this value is the standard of **SPVP**. To clarify, if we need high performance of the classifier, the value of **SPVP** should be insensitive to external and internal factors. When the value of **SPVP** is small, indicating that point vector in feature space is stable, as shown in Fig. 23, the classifier will be effective, with high efficiency. Conversely, when the value of **SPVP** is increased, showing that the point vector is very sensitive, the performance will be ineffectual.

The image intensity F_1 and contrast F_3 were varied as illustrated in Fig. 22-b since the photon energy is affected by variation of visible light intensity, therefore the value of pixels in digital image or multispectral image is certainly changed and then all features value based on GLI or GLCM will be instable under external and internal factors that we discussed in section II.

It is seen in Fig. 23-b that there are small variations from point to point; this fluctuation occurs because the emissivity is changeable at constant temperature (see Fig. 4 and [18]). It should be noted that the spectral band of the IC ranges from 8 μm to 14 μm, and the spectral band of the visible light ranges from 0.38 μm to 0.74 μm, which means that it will never influence the infrared image because the IC starts to sense from 8 μm to 14 μm. Likewise, take two points from Fig. 23-b (e.g., at 360 lux $x_1 = 27.1$ and at 422 lux

$x_2 = 27.9$), and subtract the two points from each other ($27.9 - 27.1 = 0.8$); this means that the point vector in feature space is more stable compared to the previous works as listed in Table 9. In section V- *A*, we demonstrated the ability of

infrared radiation to pass the thin layer of coal, i.e., "grinded coal"; see (Fig. 15-c), (Fig. 15-d), (Fig. 16-c), (Fig. 16-d), (Fig. 17-c) and (Fig. 17-d). Furthermore, the proposed method effectively achieved a high accuracy of 97.83% with a large test set, containing 2200 infrared images, although the visible light intensity and surface temperature of the samples were different. Conclusively, the proposed method is robust and more reliable compared to the different approaches as listed in Table 9.

VI. CONCLUSION AND FUTURE WORK

A method utilizing an infrared camera to separate gangue from coal was presented in this paper. The emissivity also played an important role; it is also a fundamental part of this investigation. We converted the disparity in emissivity into images and then extracted texture features based on the GLI, GLCM and extracted *Cb* from the YCbCr color spaces. The purpose of this step is to obtain one feature on which to rely for the classification of coal and gangue.

This work not only can be applied in industrial mining but also can be exploited for whole materials or product classification systems that can withstand temperatures from approximately 30°C to 90°C, including food industries, plastic industries, etc.

Overall, infrared images are more reliable than ordinary images or multispectral images, particularly in coal and gangue separation. This technology is useful and effective owing to its ability to address the problems of large data and time complexity that occur for ordinary images by employing *Cb*, which was extracted from the YCbCr color space as key factor for the identification process in the production lines of mining factories. Conclusively, the proposed technique is feasible and efficient.

In the future work, we will apply this technology on real conditions work in production lines of mining factories. Furthermore, this technology will be incorporated with manipulator in order to study and analyze time response of the manipulator to the data that send from the infrared camera and then study the economic benefits for this methodology in the industrial mining field.

IMAGE COURTESY
REFAT M.A. ESHAQ declares the follows:

- Figures 3, 5, and 7 were captured by my own camera
- Figures 8, 15, 16, 17, 18 and 23 were captured by laboratory's infrared camera (Ti32, FLUKE, Washington, USA, SN: Ti32-11010202)
- Figure 22 was taken by laboratory's industrial digital camera (MER-230-168U3M, GET CAMERAS, Eindhoven, Netherlands, SN:NG0190040085)
- Figures 4, 11 and 12 were created and designed by us depend the laws of heat transfer and gas dynamics [14], [20]
- The light intensity was measured by laboratory's light meter (TES-1334A, TES, Taipei, Taiwan SN: 191000981)

"Whole work besides figures in this paper were performed and saved ©by my own computer (ZBook 15 G2, HP, Intel(R) Core (TM) i7-4810MQ CPU @ 2.8 GHz, SN: CND5386L7T)"

REFERENCES

[1] B. Dudley, "BP statistical review of world energy," *BP Stat. Rev.*, London, U.K., Tech. Rep., Aug. 2019, vol. 6.

[2] J. Sun and B. Su, "Coal–rock interface detection on the basis of image texture features," *Int. J. Mining Sci. Technol.*, vol. 23, no. 5, pp. 681–687, Sep. 2013.

[3] K. Liu, X. Zhang, and Y. Chen, "Extraction of coal and gangue geometric features with multifractal detrending fluctuation analysis," *Appl. Sci.*, vol. 8, no. 3, p. 463, 2018.

[4] F. Hu, M. Zhou, P. Yan, K. Bian, and R. Dai, "Multispectral imaging: A new solution for identification of coal and gangue," *IEEE Access*, vol. 7, pp. 169697–169704, 2019.

[5] H. Yaqun, H. Jingfeng, Z. Nianxin, C. Bo, and L. Haonan, "Research on identification of coal and waste rock based on PCA and GA-ANN," *Energy*, vol. 3, no. 255, p. 255, 2010.

[6] K. Gao, C. Du, H. Wang, and S. Zhang, "An efficient of coal and gangue recognition algorithm," *Int. J. Signal Process., Image Process. Pattern Recognit.*, vol. 6, no. 4, pp. 345–354, 2013.

[7] M.-H. Zhao, S. Ma, and D.-X. Zhao, "Image processing based on gray information in sorting system of coal gangue," in *Proc. 10th Int. Conf. Intell. Hum.-Mach. Syst. Cybern. (IHMSC)*, vol. 2, Aug. 2018, pp. 81–83.

[8] M.-H. Zhao, "Intelligent sorting system of coal gangue with machine vision," in *Proc. 10th Int. Conf. Intell. Hum.-Mach. Syst. Cybern. (IHMSC)*, Aug. 2018, pp. 4–7.

[9] L. Su, X. Cao, H. Ma, and Y. Li, "Research on coal gangue identification by using convolutional neural network," in *Proc. 2nd IEEE Adv. Inf. Manage., Communicates, Electron. Autom. Control Conf. (IMCEC)*, May 2018, pp. 810–814.

[10] M. Li and K. Sun, "An image recognition approach for coal and gangue used in pick-up robot," in *Proc. IEEE Int. Conf. Real-Time Comput. Robot. (RCAR)*, Aug. 2018, pp. 501–507.

[11] W. Gomez, W. C. A. Pereira, and A. F. C. Infantosi, "Analysis of co-occurrence texture statistics as a function of gray-level quantization for classifying breast ultrasound," *IEEE Trans. Med. Imag.*, vol. 31, no. 10, pp. 1889–1899, Oct. 2012.

[12] R. C. Gonzalez and R. E. Woods, "Image segmentation 1' and 'Feature extraction," in *Digital Image Processing*. London, U.K.: Pearson Education, 2018.

[13] Mathworks. (1994). Hyperparameter optimization in classification learner app. The MathWorks, Inc, Natick, MA, USA. Accessed: 2020. [Online]. Available: https://www.mathworks.com/help/stats/hyperparameter-optimization-in-classification-learner-app.html

[14] Y. Cengel and A. Ghajar, "Fundamentals of convection 'external forced convection' and 'fundamentals of thermal radiation," in *Heat and Mass Transfer: Fundamentals and Applications*. New York, NY, USA: McGraw-Hill, 2015.

[15] M. Teena and A. Manickavasagan, "Thermal infrared imaging," in *Imaging with Electromagnetic Spectrum*. Springer, 2014, pp. 147–173.

[16] R. Vadivambal and D. S. Jayas, "Applications of thermal imaging in agriculture and food industry—A review," *Food Bioprocess Technol.*, vol. 4, no. 2, pp. 186–199, Feb. 2011.

[17] A. A. Gowen, B. K. Tiwari, P. J. Cullen, K. McDonnell, and C. P. O'Donnell, "Applications of thermal imaging in food quality and safety assessment," *Trends Food Sci. Technol.*, vol. 21, no. 4, pp. 190–200, Apr. 2010.

[18] S. R. Cone, T. McKay, C. Lapszynski, B. M. Rodriguez, and H. J. Mitchell, "Temperature emissivity separation using optimized atmospheric water band regions," in *Proc. IEEE Aerosp. Conf.*, Mar. 2017, pp. 1–7.

[19] V. Bernard, E. Staffa, V. Mornstein, and A. Bourek, "Infrared camera assessment of skin surface temperature—Effect of emissivity," *Phys. Medica*, vol. 29, no. 6, pp. 583–591, Nov. 2013.

[20] T. D. Eastop and A. Mc Conkey, *Applied Thermodynamics for Engineering Technologies*. London, U.K.: Pearson, 1993.

[21] M. Fathallah, F. Abdelhedi, and N. Derbel, "A synchronizing second order sliding mode control applied to decentralized time delayed multi-agent robotic systems: Stability proof," *Adv. Sci., Technol. Eng. Syst. J.*, vol. 2, no. 3, pp. 160–170, 2017.

[22] K. H. B. Ghazali, J. Ma, R. Xiao, and S. A. Lubis, "An innovative face detection based on YCgCr color space," *Phys. Procedia*, vol. 25, pp. 2116–2124, 2012.

[23] R. Starosolski, "New simple and efficient color space transformations for lossless image compression," *J. Vis. Commun. Image Represent.*, vol. 25, no. 5, pp. 1056–1063, Jul. 2014.

[24] C.-W. Hsu, C.-C. Chang, and C.-J. Lin, "A practical guide to support vector classification," Tech. Rep., 2003.

[25] A. Jindal, A. Dua, K. Kaur, M. Singh, N. Kumar, and S. Mishra, "Decision tree and SVM-based data analytics for theft detection in smart grid," *IEEE Trans. Ind. Informat.*, vol. 12, no. 3, pp. 1005–1016, Jun. 2016.

[26] Z. Yin and J. Hou, "Recent advances on SVM based fault diagnosis and process monitoring in complicated industrial processes," *Neurocomputing*, vol. 174, pp. 643–650, Jan. 2016.

[27] L. Shen, H. Chen, Z. Yu, W. Kang, B. Zhang, H. Li, B. Yang, and D. Liu, "Evolving support vector machines using fruit fly optimization for medical data classification," *Knowl.-Based Syst.*, vol. 96, pp. 61–75, Mar. 2016.

[28] M. A. Nanda, K. B. Seminar, D. Nandika, and A. Maddu, "A comparison study of kernel functions in the support vector machine and its application for termite detection," *Information*, vol. 9, no. 1, p. 5, 2018.

[29] C. Qi and X. Tang, "Slope stability prediction using integrated Metaheuristic and machine learning approaches: A comparative study," *Comput. Ind. Eng.*, vol. 118, pp. 112–122, Apr. 2018.

[30] L. H. Hamel, *Knowledge Discovery With Support Vector Machines*. Hoboken, NJ, USA: Wiley, 2011.

[31] A. Keshavarz, H. Akhondzadeh, M. Sayyafzadeh, and M. Zagar, "Enhanced gas recovery techniques from coalbed methane reservoirs," Tech. Rep., 2018.

ERYI HU received the Ph.D. degree from the School of Mechanical Engineering, Huazhong University of Science and Technology, Wuhan, China. He is currently an Associate Professor and the Director of the School of Mechanical and Electrical Engineering, Mine Robot Research Institute, China University of Mining and Technology, Xuzhou, China. His research interests include mining robot design, machine vision, and optical measurement technique.

MENGGANG LI received the master's degree in mechanical engineering from the China University of Mining and Technology, Xuzhou, China, in 2017, where he is currently pursuing the Ph.D. degree in vehicle engineering. His research interests include perception, positioning, and navigation for special robots.

REFAT MOHAMMED ABDULLAH ESHAQ was born in Sana'a, Yemen, in 1993. He received the B.S. degree in mechanical engineering from the Arab Academy for Science, Technology and Maritime Transport, Alexandria, Egypt, in 2018. He is currently pursuing the M.S. degree in mechanical and electrical engineering, his major area of study is mechanical and electronic engineering, China University of Mining and Technology, Xuzhou, China. His research interests include the heat transfer, gas dynamics, and fluid mechanics application in intelligent industry. In 2018, he was awarded a scholarship by the China Scholarship Council (CSC) to resume postgraduate studies.

MURAD SALEH ALFARZAEAI received the bachelor's degree in computer science and engineering from the Faculty of Computer Science and Engineering, Hodeidah University, Hodeidah, Yemen, in 2006, and the master's degree in computer science from the Faculty of Computer Science, Amman Arab University, Amman, Jordan, in 2013. He is currently pursuing the Ph.D. degree with the School of Computer Science and Technology, China University of Mining and Technology, China. His research interests are in neural networks and deep learning.

● ● ●